JOURNAL OF APPLIED ELECTROCHEMISTRY **27** (1997) 1328–1332

Effect of temperature on performance of $LaNi_{4.76}Sn_{0.24}$ metal hydride electrode

G. ZHENG, B. N. POPOV, R. E. WHITE

Department of Chemical Engineering, University of South Carolina, Columbia, SC 29208, USA

Received 12 December 1996; revised 27 June 1997

The effect of temperature on the performance of a $LaNi_{4.76}Sn_{0.24}$ metal hydride electrode was investigated in the temperature range of 0 to 50 °C. The electrode showed a maximum discharge capacity at 25 °C. The total resistance increases with a decrease of temperature from 50 °C to 0 °C. The apparent activation enthalpies at different states of charge were determined by evaluating the polarization resistance at different temperatures. It was found that the apparent activation enthalpy is an indicator of the relative reaction rate of the charge-transfer reaction and hydrogen absorption.

Keywords: *metal hydride*, *capacity*, *temperature*, *performance*, *enthalpy*

List of symbols

A	a constant in Equation 4
C	capacitance (F)
F	Faraday's constant (96 487 C mol^{-1})
$\Delta_{ab}\overline{H}^0$	enthalpy change for hydrogen absorption (kJ mol^{-1})
$\Delta_r H^*$	apparent activation enthalpy (kJ mol^{-1})
$\Delta_r H^=$	Activation enthalpy for the charge-transfer reaction (kJ mol^{-1})
i	current density per unit of mass (A g^{-1})
i_0	exchange current density per unit of mass (A g^{-1})
j	$\sqrt{-1}$, imaginary number
Q_{cpe}	$1/Y(j\omega)^n$ $(0 < n < 1)$, constant phase element (Ω)
R	gas constant, 8.3143 J mol^{-1} K^{-1}
R_{el}	electrolyte resistance (Ω g)
R_{cp}	current collector to pellet contact resistance (Ω g)
R_p	polarization resistance (Ω g)
R_{pp}	particle to particle contact resistance (Ω g)
R_t	total resistance determined from linear polarization curves (Ω g)
R_w	Warburg impedance (Ω g)
T	temperature (K)
Y	a capacitive component ($s^n\Omega^{-1}$)

Greek letters

η	overpotential (V)
ω	angular frequency (rad s^{-1})

1. Introduction

It is important for metal hydride batteries to operate satisfactorily over a wide range of temperatures [1, 2]. Typically, for the metal–hydride battery the best performance is obtained between 0 and 40 °C [2, 3]. The discharge performance of metal hydride batteries are affected more at low temperatures than at high temperatures [3]. Also, the temperature effects on discharge performance of the metal hydride battery were found to be more pronounced at higher discharge rates [3]. However, this is not true for all kinds of metal–hydride alloys. For example, a rapid decrease of capacity was observed for $La_{1-x}Zr_xNi_5$ ($x = 0.1$ and 0.2) when the temperature was increased from 0 to 40 °C. On the other hand, for $La_{1-x}Zr_xNi_{4.5}Al_{0.5}$ the discharge capacity showed a maxima at 20 °C between −20 and 40 °C [4].

There is also disagreement in the literature regarding the temperature effects on hydrating reaction kinetics. Two opposite effects of temperature on the reaction rate were observed. One is that the hydrating reaction rate increases with increase of temperature and another is that the rate decreases with increase of the temperature [5].

In the present study, the performance of $LaNi_{4.76}Sn_{0.24}$ electrode was investigated at 50, 35, 25, 15 and 0 °C. The discharge capacities were measured for different discharge rates as a function of temperature. Linear polarization and electrochemical impedance spectroscopy techniques were used to determine the total resistance, polarization resistance and ohmic resistance of the electrodes. The apparent activation enthalpies were determined as a function of state of charge of the electrodes.

2. Experimental details

The alloy $LaNi_{4.76}Sn_{0.24}$ was first crushed and ground mechanically. The resulting powder was passed through a 230 mesh sieve, which gave a particle size of less than 63 μm. Next, a pellet electrode was prepared by mixing the alloy with PTFE powder (5% w/o) and then pressing the material in a cylindrical

0021-891X

press (5/16 inch diam.) at 300 °C. The pellet electrode was then inserted between two pieces of plexiglass with small holes on each side. A piece of Pt gauze was placed on each side of the electrode and served as counter electrode. The pellet electrode was immersed in the test cell and filled with a 6 M KOH electrolyte solution. Experiments were carried out using a Hg/HgO reference electrode. Good electrical connection to the pellet electrode was achieved by threading a piece of nickel wire through the nickel mesh and then pressing the nickel mesh and the wire together to ensure good electrical contact.

Prior to each experiment, the pellet electrode was activated by cycling. The experimental procedure was performed as follows. The electrode was charged under a constant current mode until the hydrogen content reached its saturated value. After the open circuit potential (o.c.p.) stabilized, linear polarization and electrochemical impedance spectroscopy experiments were carried out. Then the electrode was discharged for a certain period of time and the same measurements as above were conducted. This procedure was repeated until the electrode was discharged to reach the cut-off potential (−0.6 V vs Hg/HgO). The experiments were conducted using the model 342C SoftCorr system with EG&G PAR potentiostat/galvanostat model 273A.

3. Results and discussion

To examine the effect of temperature on the alloy discharge performance, the electrode was discharged at different temperatures from the fully charged state. The discharge curves obtained at 50, 35, 25, 15 and 0 °C using two discharge current densities are shown in Figs 1 and 2. The current density of 27.3 mA g^{-1} corresponds to a 0.1 C rate at 25 °C. The discharge capacity is defined for cut-off potential of −0.6 V vs Hg/HgO reference electrode. In both Figures, the initial discharge potentials are more negative at high

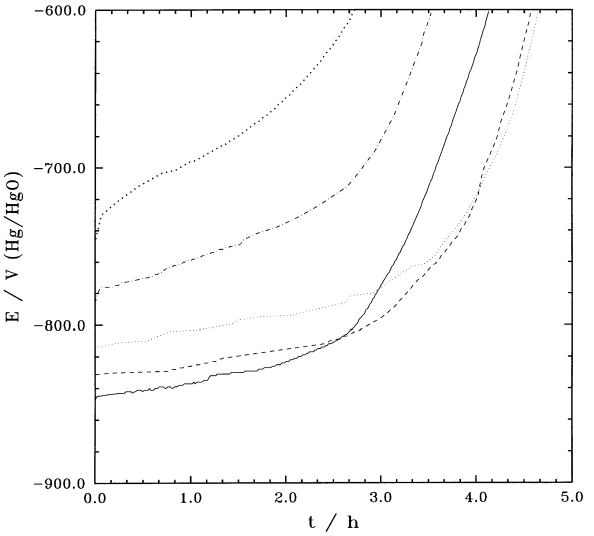

Fig. 2. Discharge curves obtained at different temperatures. Discharge c.d. 54.7 mA g^{-1}. Key: (——) 50 °C; (– – – –) 35 °C; (·····) 25 °C; (– · – · –) 15 °C; (· · · · ·) 0 °C.

temperatures indicating that the electrode internal resistances decrease with the increase of the temperature. The effect of temperature on the initial discharge potentials are more pronounced at high discharge rates. As shown in Fig. 1, an initial potential drop of 40 mV (from −880 to −840 mV vs Hg/HgO) was observed at a 27.3 mA g^{-1} rate when temperature was changed from 50 to 0 °C. On the other hand, when a higher discharge rate of 54.7 mA g^{-1} was used, the initial potential dropped from −845 mV at 50 °C to 740 mV at 0 °C, which is a 105 mV difference. The electrode reaches the cut-off potential (−0.6 V vs Hg/HgO) faster at high and low temperatures than at intermediate temperatures. The largest discharge capacity was observed at 25 °C.

Figure 3 shows the discharge capacity as a function of temperature at two discharge rates. The discharge capacity of the electrode was moderately affected at high temperatures, while it decreased more

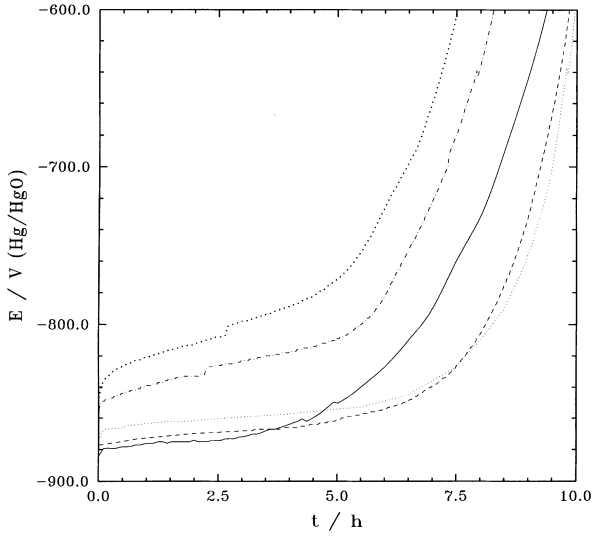

Fig. 1. Discharge curves obtained at different temperatures. Discharge c.d. 27.3 mA g^{-1}. Key: (——) 50 °C; (– – – –) 35 °C; (·····) 25 °C; (– · – · –) 15 °C; (· · · · ·) 0 °C.

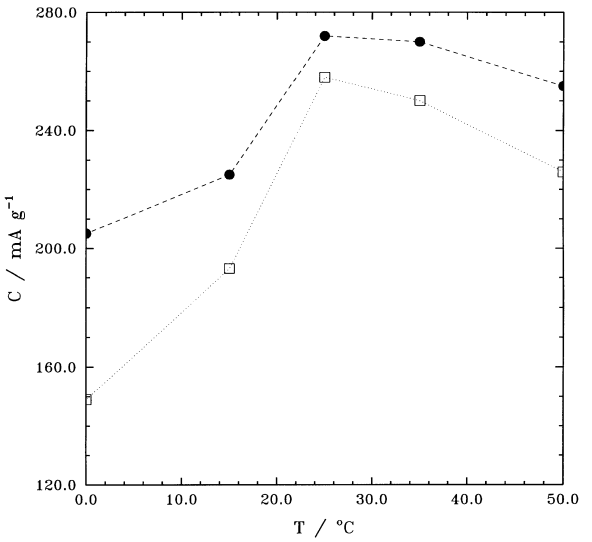

Fig. 3. Discharge capacity against temperatures at two different discharge current densities: (●) 27.3 mA g^{-1} and (□) 54.6 mA g^{-1}.

significantly at the lower discharge temperatures. For instance, at a 0.1 C rate when the temperature was increased from 25 to 50 °C, the discharge capacity was decreased by 6% compared with a decrease of 25% when the temperature was decreased from 25 to 0 °C. The decrease of the discharge capacity at low temperatures was due to an increase in the internal resistance of the electrode. The capacity loss at high temperature was probably due to the effect of self-discharge. Because the experiments were carried out in an open cell, the observed capacity loss at higher temperatures was also result of an increase in the equilibrium pressure at higher temperatures [6–8].

The linear polarization measurements were carried out using potentiodynamic method at scan rate of $10\,\mathrm{mV\,s^{-1}}$. The typical linear polarization curves at a 100% state of charge for five different temperatures are presented in Fig. 4. The slopes of the curves shown in Fig. 4 increase with a decrease of temperature. This indicates that the electrode resistance is higher at lower temperatures. The total resistances determined from linear polarization curves at different temperatures are plotted as a function of state of charge in Fig. 5.

The total resistance which was determined from the linear polarization is equal to the polarization resistance (R_p) only when the electrode ohmic resistance is negligible [9, 10]. In such a case, the exchange current density of the electrode may be determined by

$$R_p = RT/F\bar{i}_0 = \eta/i \qquad (1)$$

However, when the ohmic resistance is not negligible, then Equation 1 will estimate sum of the polarization resistance and ohmic resistance. Consequently, the exchange current density will be underestimated. EIS enables a determination of the polarization resistance and an evaluation of the exchange current density without the interference of any of the ohmic resistances related to alloy particle to particle contact resistance and current collector to pellet contact resistance.

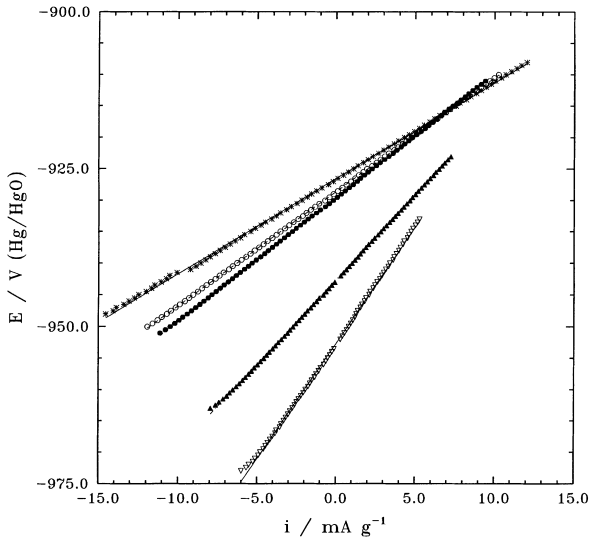

Fig. 4. Linear polarization curves at 100% state of charge at obtained different temperatures. Scan rate, $v = 10\,\mathrm{mV\,s^{-1}}$. Key: (∗) 50 °C; (○) 35 °C; (●) 25 °C; (▲) 15 °C; (▽) 0 °C.

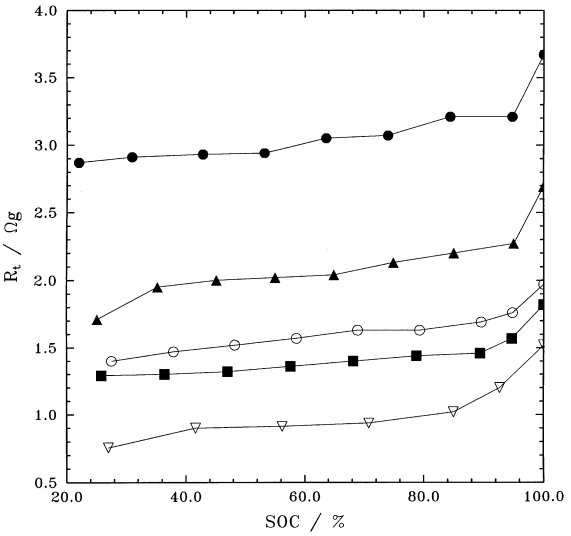

Fig. 5. Total resistance as a function of state of charge at different temperatures: (●) 0 °C; (▲) 15 °C; (○) 25 °C; (■) 35 °C; (▽) 50 °C.

EIS experiments were carried out at different stages of charge. The impedance data generally covered the frequency range from 0.002 Hz to 100 kHz with an ac voltage signal of ± 5 mV, which ensured the electrode system to be under minimum perturbation. According to Kuriyama *et al.* [11–13] the total resistance of the electrode may be contributed from the following resistances: (i) the electrolyte resistance (R_{el}); (ii) the resistance between the current collector and the electrode pellet (R_{cp}); and (iii) the alloy particle to particle contact resistance (R_{pp}); and (iv) the polarization resistance (R_p). The polarization resistance is related to the electrode reaction on the alloy surface and is inversely proportional to the active surface area. The corresponding equivalent circuit is shown in Fig. 6, where R_w is the Warburg resistance, C is the capacitance and Q_{cpe} is the constant phase element (CPE) [14]. The Nyquist plots for the fully charged electrode at different temperatures are presented in Fig. 7.

As shown in Fig. 7, the total impedance decreases with the increase of temperature, which is consistent with the linear polarization results. Two semicircles are observed in each curve. According to Kuriyama *et al.* [11–13] the semicircle at the low frequency region represents the polarization resistance while the semicircle at the high frequency region represents the contact resistance between current collector and electrode pellet. A third semicircle exists between these two semicircles which represents the alloy particle-to-particle contact resistance. At low states of charge (< 20%), however, these semicircles are not distinguishable. The electrode resistive components were determined from the EIS data by applying the

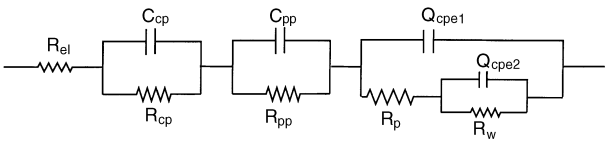

Fig. 6. An equivalent circuit for metal–hydride electrode.

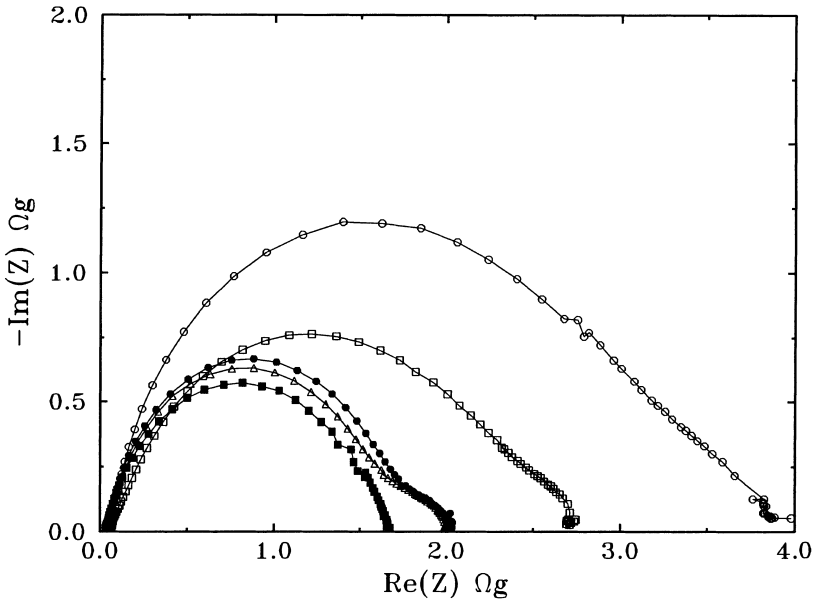

Fig. 7. Nyquist plots at 100% state of charge obtained at different temperatures: (○) 0 °C; (□) 15 °C; (●) 25 °C; (△) 35 °C; (■) 50 °C.

equivalent circuit shown in Fig. 6. The results were fitted by using ZView® (Scribner Associates, Inc.). The resultant ohmic resistance (the sum of current collector to pellet contact resistance and particle to particle contact resistance) and polarization resistance are presented in Figs 8 and 9, respectively. As shown in these figures, the ohmic resistance and the polarization resistance of the electrode increase with an increase of the state of charge. However, the ohmic resistance is larger than the polarization resistance at the same state of charge of the electrode.

The main electrode reactions occurring at the metal hydride electrode are

$$M + H_2O + e^- \rightleftharpoons MH_{ads} + OH^- \quad (2)$$

$$MH_{ads} \rightleftharpoons MH_{abs} \quad (3)$$

where H_{ads} and H_{abs} represent the hydrogen atom adsorbed on the surface and absorbed in the electrode, respectively. The apparent activation enthalpy $(\Delta_r H^*)$ of the charge transfer reaction (Equation 2) occurring on the metal–hydride surface can be determined from temperature data by using the slope of Equation 4 [11]:

$$\log\left(\frac{T}{R_p}\right) = -\frac{\Delta_r H^*}{2.3RT} + A \quad (4)$$

where R is the gas constant and A is a constant. The polarization resistances (R_p) presented in Fig. 9 were used to plot the dependence of $\log(T/R_p)$ vs $1/T$ in Fig. 10. The apparent activation as shown in Fig. 11 increases when the state of charge is decreased from 100% to 80%. At a state of charge between 40% and 80%, $\Delta_r H^*$ was almost independent of the state of charge and it starts to increase again when the state of charge decreases from 40% to 10%. Kuriyama *et al.* [13] found that the apparent activation enthalpy and the polarization resistance estimated at 90% state of

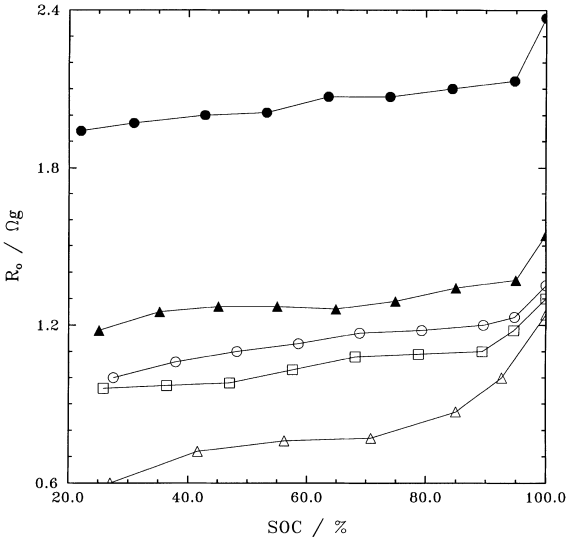

Fig. 8. Ohmic resistance as a function of state of charge at different temperatures: (●) 0 °C; (▲) 15 °C; (○) 25 °C; (□) 35 °C; (△) 50 °C.

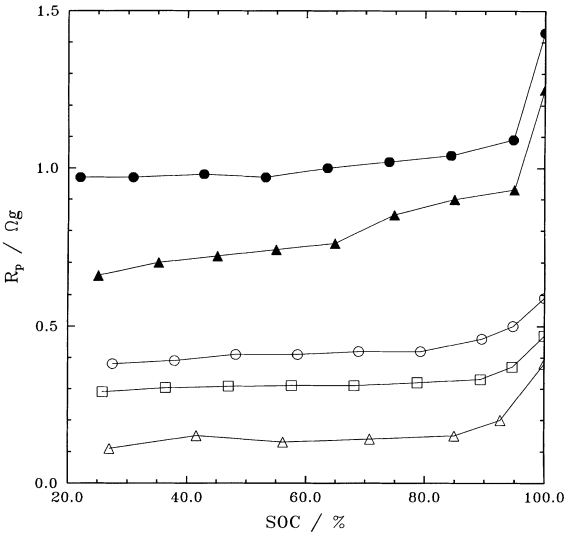

Fig. 9. Polarization resistance as a function of state of charge at different temperatures: (●) 0 °C; (▲) 15 °C; (○) 25 °C; (□) 35 °C; (△) 50 °C.

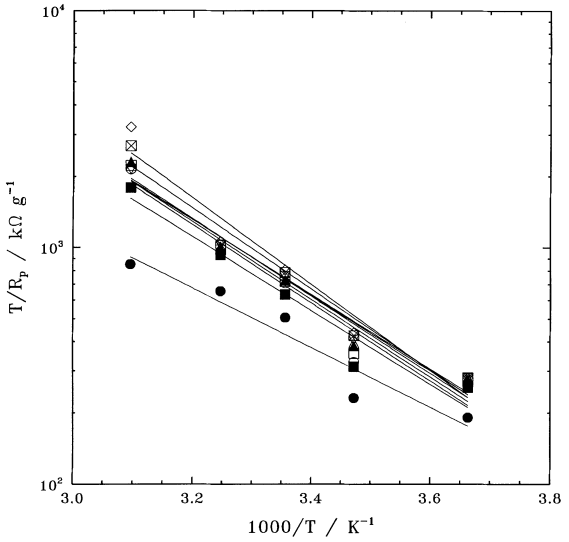

Fig. 10. T/R_p against $1000/T$ at different states of charge: (●) 100%; (■) 90%; (○) 80%; (□) 70%; (▲) 60%; (△) 50% (▽) 40%; (⊠) 30%; (◇) 25%.

charge increase with number of cycles and they have concluded that the apparent activation enthalpy is an indicator of the surface activity. According to our results the polarization resistance increases with an increase of the state of charge. Thus, if the apparent activation enthalpy is an indicator of the surface activity for Reaction 2, then the dependence of $\Delta_r H^*$ upon state of charge should be consistent with the dependence of polarization resistance upon the state of charge. This is due to the fact that the polarization resistance is the reaction resistance for Reaction 2. According to our results, the change of $\Delta_r H^*$ is opposite to that of R_p. The results can be explained by taking into account that the apparent activation enthalpy ($\Delta_r H^*$) is related to the activation enthalpy for Reaction 2 ($\Delta_r H$), and the enthalpy change for the absorption Reaction 3 ($\Delta_{ab}\overline{H}^0$) according to Equation 5:

$$\Delta_r H^* = \Delta_r H^{=} - \alpha\Delta_{ab}\overline{H}^0 \qquad (5)$$

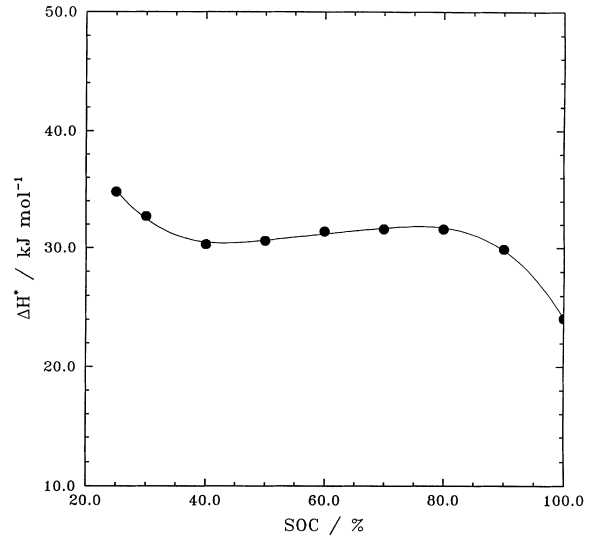

Fig. 11. Apparent activation enthalpy as a function of state of charge.

Thus, at high states of charge due to the saturation of the alloy with hydrogen, the second term on the right hand of Equation 5 is comparable with the first term which results the values of $\Delta_r H^*$ to be small. At intermediate states of charge, both $\Delta_r H^{=}$ and $\Delta_{ab}\overline{H}^0$ are almost constant, causing $\Delta_r H^*$ to be almost independent of state of charge. At low states of charge, $\Delta_r H^*$ is dominated by $\Delta_r H^{=}$ since the electrode is far from the saturation. According to our results, the apparent activation enthalpy is not an indicator of the surface activity as claimed by Kuriyama *et al.* [13] rather it is an indicator of the rate of hydrogen absorption and the relative reaction rate of the charge-transfer reaction occurring on the surface of the electrode.

4. Conclusion

The performance of $LaNi_{4.76}Sn_{0.24}$ was studied in the temperature range of 0 to 50 °C. The observed loss in capacity at low temperatures is probably due to the high internal resistance, while the observed loss at high temperatures is caused by the self-discharge of the electrode and high equilibrium hydrogen pressure at high temperatures. The apparent activation enthalpies at different states of charge were determined by measuring the polarization resistances at different temperatures. It was found that the apparent activation energy is an indicator of the relative reaction rate of the charge-transfer reaction occurring at the interface and an indicator for the rate of hydrogen absorption.

Acknowledgement

Financial support by the Exploratory Technology Research (ETR) Program, which is supported by the Office of Transportation Technologies (OTT) of the US Department of Energy (DOE), subcontract 4614610, is acknowledged gratefully.

References

[1] F. R. Kalhammer, A. Kozawa, C. B. Moyer and B. B. Owens, *Electrochem. Soc. Interface* **1** (1995) 26.
[2] P. D. Bennet, K. R. Bullock and M.E. Fiorino, *Electrochem. Soc. Interface* **4** (1995) 26.
[3] D. Linden, *in* 'Handbook of Batteries', 2nd edn (edited by D. Linden), McGraw-Hill, New York (1995), p. 33.1.
[4] T. Sakai, H. Miyamuru, N. Kuriyama, A. Kato, K. Oguro and H. Ishikawa, *J. Electrochem. Soc.* **137** (1990) 795.
[5] X. Wang and S. Suda, *J. Hydrogen Energy* **17** (1992) 139.
[6] G. Bronoel, J. Sarradin, M. Bonnemay, A. Percheron, J. C. Achard and L. Schlapabach. *ibid.* **1** (1976) 251.
[7] T. Kitamura, C. Iwakura and H. Tamura, *Electrochim. Acta* **27** (1982) 1723.
[8] H. Uchida and Y. Naragaki, *Z. Phys. Chem.* **179** (1993) 93.
[9] G. Zheng, B. N. Popov and R. E. White, *J. Electrochem. Soc.* **143** (1996) 834.
[10] *Idem*, *ibid.* **143** (1996) 435.
[11] N. Kuriyama, T. Sakai, H. Miyamura, I. Uehara and H. Ishikawa, *J. Alloys Compd.* **202** (1993) 183.
[12] N. Kuriyama, T. Sakai, H. Miyamura, I. Uehara and H. Ishikawa, *J. Alloys Compd.* **192** (1993) 161.
[13] N. Kuriyama, T. Sakai, H. Miyamura, I. Uehara, and H. Ishikawa, *J. Electrochem. Soc.* **139** (1992) L72.
[14] J. R. Macdonald (Ed.), 'Impedance Spectroscopy, Emphasizing Solid Materials and Systems', J. Wiley & Sons, New York (1987).